CHEMISTRY OF MATERIALS
Cite This: Chem. Mater. 2019, 31, 1946−1955
Article
pubs.acs.org/cm

Molecular Insights into Carbon Dioxide Sorption in Hydrazone-Based Covalent Organic Frameworks with Tertiary Amine Moieties

Kerstin Gottschling,[†,‡,§,∥] Linus Stegbauer,[†,‡,§] Gökcen Savasci,[†,‡,∥] Nathan A. Prisco,[⊥] Zachariah J. Berkson,[⊥] Christian Ochsenfeld,[‡,∥] Bradley F. Chmelka,[⊥] and Bettina V. Lotsch*[,†,‡,§,∥]

[†]Max Planck Institute for Solid State Research, Heisenbergstraße 1, 70569 Stuttgart, Germany
[‡]Department of Chemistry, University of Munich (LMU), Butenandtstraße 5-13, 81377 München, Germany
[§]Nanosystems Initiative Munich (NIM), Schellingstraße 4, 80799 München, Germany
[∥]Center for Nanoscience, Schellingstraβe 4, 80799 München, Germany
[⊥]Department of Chemical Engineering, University of California, Santa Barbara, Santa Barbara, California 93106, United States

Supporting Information

ABSTRACT: Tailorable sorption properties at the molecular level are key for efficient carbon capture and storage and a hallmark of covalent organic frameworks (COFs). Although amine functional groups are known to facilitate CO_2 uptake, atomistic insights into CO_2 sorption by COFs modified with amine-bearing functional groups are scarce. Herein, we present a detailed study of the interactions of carbon dioxide and water with two isostructural hydrazone-linked COFs with different polarities based on the 2,5-diethoxyterephthalohydrazide linker. Varying amounts of tertiary amines were introduced in the COF backbones by means of a copolymerization approach using 2,5-bis(2-(dimethylamino)-ethoxy)terephthalohydrazide in different amounts ranging from 25 to 100% substitution of the original DETH linker. The interactions of the frameworks with CO_2 and H_2O were comprehensively studied by means of sorption analysis, solid-state NMR spectroscopy, and quantum-chemical calculations. We show that the addition of the tertiary amine linker increases the overall CO_2 sorption capacity normalized by the surface area and of the heat of adsorption, whereas surface areas and pore size diameters decrease. The formation of ammonium bicarbonate species in the COF pores is shown to occur, revealing the contributing role of water for CO_2 uptake by amine-modified porous frameworks.

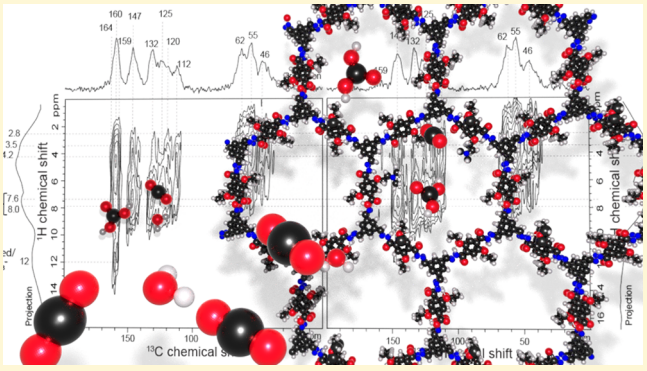

INTRODUCTION

Covalent organic frameworks (COFs) are a recently developed class of porous polymers with high chemical and thermal stability and well-defined crystal structures. COFs are promising for a range of applications, for example, in gas storage and separation,[1−3] optoelectronics,[4,5] and energy conversion.[6,7] COFs are formed by condensation reactions of organic linkers that are covalently bound under reversible conditions, which provides a mechanism of error correction.[8] All but a few COFs reported to date have two-dimensional (2D) network topologies, where the COF sheets are held together in the third dimension by noncovalent van der Waals interactions. The structure of COFs and their versatility allows for engineering these systems and their properties in a targeted manner.[9−11] One way to do so is by pore-surface engineering, where the surface of preformed pores carrying specific functional sites can be further transformed postsynthetically, if desired.[12] Another possibility is to modify the organic linkers presynthetically according to the targeted properties. A linker that is suitable for diverse transformations and has been successfully used in several COF syntheses is 2,5-diethoxyterephthalohydrazide (DETH).[7,13,14] An example is the DETH-based COF-JLU4 which is synthesized by condensation with triformylphloroglucinol (TFG) and has been used in fluorescent pH sensing systems for aqueous solutions.[15] Another chemically strongly related COF containing methoxy instead of ethoxy groups in the hydrazide linker, NUS-3, has been reported for the use in mixed-matrix membranes with high H_2/CO_2 permselectivity.[16]

Utilization of functional porous solids with custom-made pores has seen a burst of activity over the past decades, specifically in the context of carbon capture and storage (CCS). Carbon dioxide emissions are known to be the major source of global warming, and in order to reduce this effect, technically viable solutions for the capture and long-term storage of the greenhouse gas CO_2 are needed and actively

Received: November 5, 2018
Revised: February 12, 2019
Published: February 13, 2019

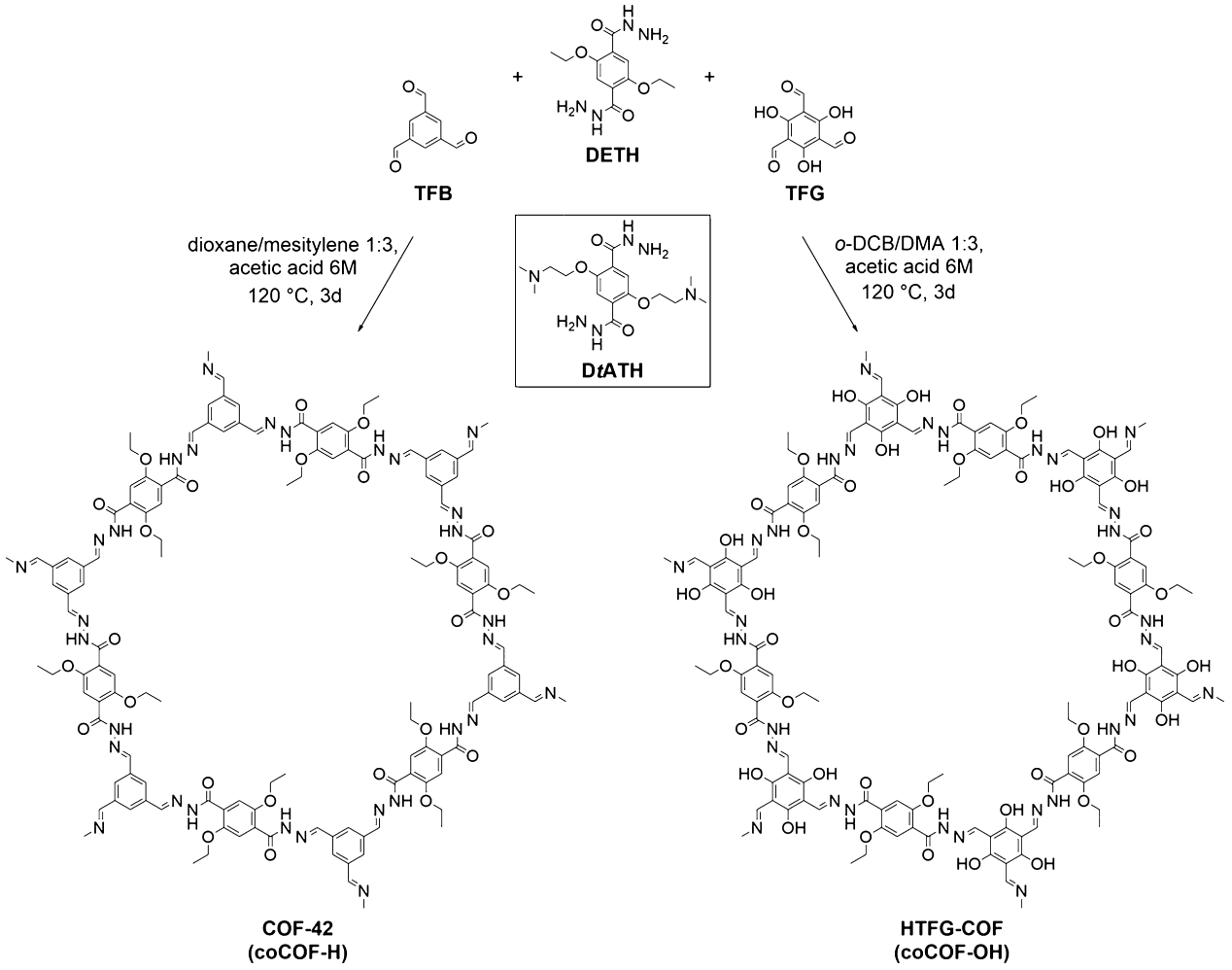

Figure 1. Synthesis of COF-42 (coCOF−H) from DETH and TFB (left) and HTFG−COF (coCOF−OH) from DETH and 2,4,6-trihydroxybenzene-1,3,5-tricarbaldehyde (TFG, right). Structure of D*t*ATH, center.

sought. The chemisorption of CO_2 into aqueous alkanolamine solutions - known as amine scrubbing - is widely practiced in the downstream processing of flue gases produced at the mega ton scale by coal-fired fire plants.[17] Primary or secondary amines form carbamates with CO_2, whereas tertiary or sterically hindered amines act as bases accepting a proton from carbonic acid formed by dissolution of CO_2 in water.[18−20] It is worth noting that unhindered alkanolamines absorb only half a mole of CO_2 per mole of amine by a zwitterion mechanism, whereas tertiary amines undergo base-catalyzed hydration of CO_2 to form bicarbonate ions which increases the theoretical capacity to 1 mol of CO_2 per mole of amine.[18] The amine solutions that are used decompose over time, and their CO_2 capturing ability decreases significantly.[21] Additional problems are the corrosivity and toxicity of these amine solutions. Key goals in CCS are high adsorption capacity and cycle stability as well as full reversibility and adequate heats of adsorption. Materials such as activated carbons,[22,23] metal−organic frameworks (MOFs),[24,25] or COFs[26,27] are, in contrast to the standard method, easy to regenerate at moderate temperatures and allow a great variety of functional designs. In this context, heterogeneous adsorbents such as COFs with precisely tunable pores decorated with functional groups are attracting increasing interest in the field. Another challenge in this context is the presence of small amounts of water, which can be competitively adsorbed by hydrophilic adsorbents, thus reducing the overall CO_2 sorption capacity.[28−30] Although mesoporous materials such as zeolites and activated carbons were already tested in pilot plants,[31,32] the potential of COFs as alternative sorbents in the CCS technology has not been explored. However, to fully develop the potential of heterogeneous sorbents in CCS, understanding the interactions that account for CO_2 adsorption at the molecular level is key.[33−35]

Here, we address this challenge by studying CO_2 sorption in tertiary amine-functionalized COFs by a combination of adsorption isotherm measurements and solid-state nuclear magnetic resonance (NMR) spectroscopy, complemented by quantum chemical calculations, obtained on B97-2/pcS-2/PBE0-D3/def2-TZVP level of theory[36−41] using the Turbomole[42,43] program package for geometries and the FermiONs++[44,45] program package for the calculation of NMR chemical shifts. DETH linker molecules were modified by insertion of a terminal tertiary amine group and integrated into two different hydrazone-linked COF systems. To adjust the linker functionalization level and study the influence of linker modification on the structural and sorption properties of the COF, a three-linker approach was developed inspired by classical copolymerization. We show that CO_2 sorption capacities as well as heats of adsorptions can be increased by

DOI: 10.1021/acs.chemmater.8b04643
Chem. Mater. 2019, 31, 1946−1955

this strategy. To the best of our knowledge, this is the first time the molecular interaction of CO_2 with a COF material was studied. CO_2 was found to adsorb at tertiary amine sites through water-mediated formation of a bicarbonate species.

RESULTS AND DISCUSSION

Synthesis and Structural Characterization. Two COF systems with different amounts of the amine-functionalized linker of 2,5-bis(2-(dimethylamino)ethoxy)-terephthalohydrazide (D*t*ATH, see Figure 1) were synthesized by a copolymerization approach using two generic COF systems.

The first system, named amine−coCOF−OH, is based on the hydrazone-linked HTFG−COF (coCOF−OH) that is synthesized by solvothermal condensation of DETH (see Figure 1) and 2,4,6-trihydroxybenzene-1,3,5-tricarbaldehyde (TFG, see Figure 1). The second system, COF-42 (coCOF−H), was synthesized similarly by condensation of DETH and 1,3,5-triformylbenzene (TFB, see Figure 1) and is referred to as amine−coCOF−H in the following.

For the synthesis of D*t*ATH-containing samples, various amounts of DETH (25, 50, 75, and 100% substitution of the original DETH linker) were substituted by the respective amount of D*t*ATH and the mixed linkers exposed to the initial COF synthesis protocol of the underlying coCOF systems coCOF−OH and coCOF−H. The solvent compositions were optimized to obtain high surface area and crystallinity in the modified samples.

COFs were characterized by Fourier transform infrared (FT-IR) spectroscopy, sorption analysis, powder X-ray diffraction (PXRD), and solid-state NMR. As seen in Figure S1, the FT-IR spectrum of coCOF−OH shows the characteristic C═O stretching vibrations of the β-ketoenamine carbonyl group at 1680 cm^{-1}. No residual aldehyde stretches are visible, indicating the complete transformation of the starting material. Comparison with the monomers corroborates the formation of the hydrazone bond. The same was found in coCOF−H as well as in the amine-containing samples. Addition of the tertiary amine linker further leads to color deepening in the samples from light yellow to orange in coCOF−OH and from orange to reddish-brown in coCOF−H as is also visible in the solid-state UV/vis absorption spectra (see Figure S3).

Solid-state 1D $^{13}C\{^1H\}$ CP-MAS NMR further supports the bond formation and linker integration in both systems. The ^{13}C NMR signals are assigned to the different carbon atoms shown schematically in Figure 2a,e as indicated by the labels in Figure 2b,f. The signals assigned to the ethoxy group were observed at 66 and 15 ppm. Amine-containing samples show additional peaks at 45 and 57 ppm (Figure 2c,d,g,h) that can be attributed to the aminoethoxy and dimethylamine groups, respectively, as corroborated by quantum chemical calculations for a model compound (see Table S3). In the molecular linker, the respective carbon center shows a ^{13}C chemical shift of 45.1 ppm (see the Supporting Information). The relative intensity of the ^{13}C NMR signal at 45 ppm increases with higher amount of amine in the synthesis mixture, consistent with greater incorporation of the amine linker into the COF framework.

PXRD confirms the formation of crystalline COF networks with unit cell dimensions being consistent with the structural models shown in Figure 3c. For coCOF−OH, a strong reflection at 3.4° and weaker ones at 5.5, 7.0, and 26.2° are assigned to the 100, 110, 200, and 001 Miller indices,

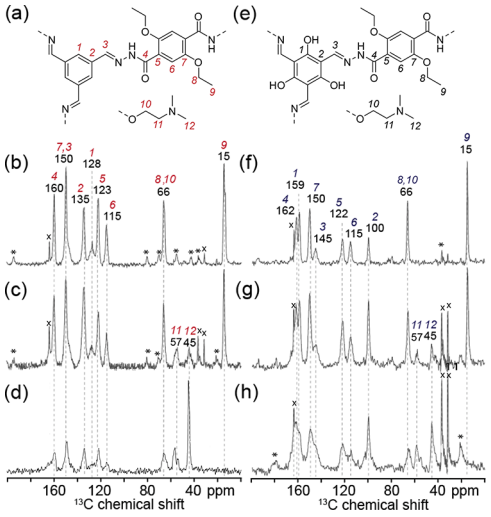

Figure 2. Schematic structural diagrams showing subsections of the (a) coCOF−H framework, (e) coCOF−OH framework, and the tertiary amine linker D*t*ATH. Solid-state one-dimensional (1D) $^{13}C\{^1H\}$ CP-MAS NMR spectra of (b−d) coCOF−H and (f−h) coCOF−OH with (b,f) 0%, (c,g) 50%, and (d,h) 100% of D*t*ATH substitution of the original DETH linker. The spectra in (b−d) and (f−h) were acquired at 11.7 T, 10 kHz MAS, 298 K, using cross-polarization contact times of 5 ms. The NMR spectrum (d) was acquired at 11.7 T, 12 kHz MAS, 298 K, and using cross-polarized contact times of 5 ms. Spinning sidebands are marked with asterisks. Distinct carbon atoms in the schematic structures in (a−e) are numbered and their associated ^{13}C NMR signals labeled accordingly in (b−d) and (f−h). The narrow signals labeled with crosses at 164, 37, and 32 ppm correspond to residual dimethylformamide and at 25 ppm to residual tetrahydrofuran.[46]

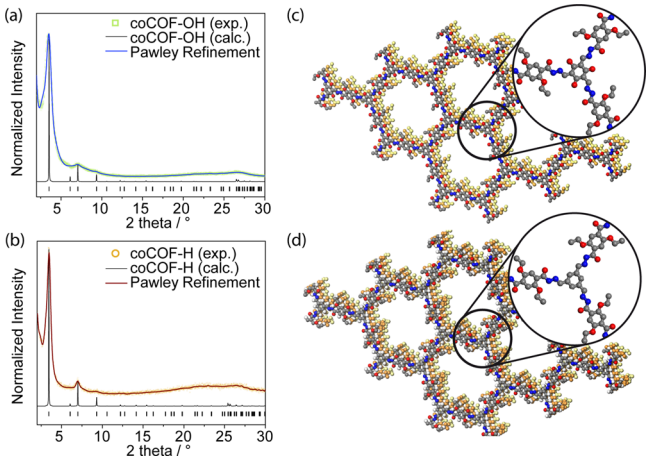

Figure 3. (a) PXRD pattern of coCOF−OH (open green squares), Pawley refined profile (blue line), and calculated XRD pattern for the idealized eclipsed (AA) stacking (black line). (b) PXRD pattern of coCOF−H (open orange circles), Pawley refined profile (red line), and calculated XRD pattern for the idealized eclipsed (AA) stacking (black line). (c) and (d) Eclipsed stacking model for coCOF−OH and coCOF−H, respectively. C, N, and O atoms are represented in gray, blue, and red, respectively. H atoms are omitted. The second and third layers are represented in orange and yellow for clarity, respectively.

respectively (see Figure 3a). The PXRD data match well with an AA eclipsed stacking structure with an interlayer distance of 3.48 Å because of $\pi-\pi$-stacking interactions (see Figure 3c). It should be noted that a lateral offset of 1.7−1.8 Å is expected

DOI: 10.1021/acs.chemmater.8b04643
Chem. Mater. 2019, 31, 1946−1955

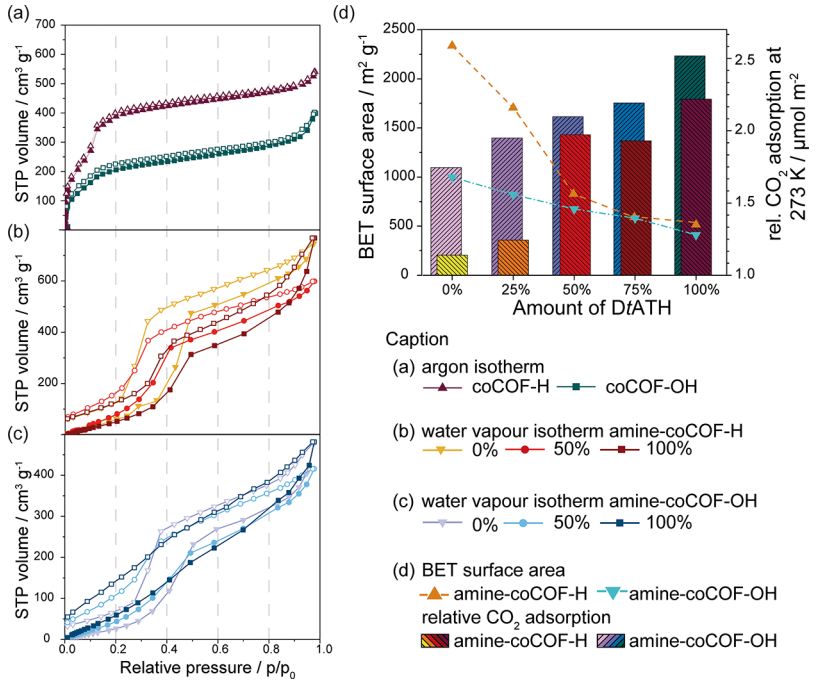

Figure 4. (a) Argon adsorption isotherms of coCOF−H (red) and coCOF−OH (blue). Water sorption at 273 K of (b) amine−coCOF−H and (c) amine−coCOF−OH with 0, 50, and 100% D*t*ATH substitution of the original DETH linker. Adsorption is represented by filled symbols, desorption by open symbols. (d) Relative CO_2 adsorption capacities at 273 K and BET surface areas of amine−coCOF−OH (blue and purple) and amine−coCOF−H (red and orange). BET surface area is indicated by triangles.

Table 1. BET Surface Areas, CO_2 Uptake at 273 K, Relative CO_2 Adsorption at 273 K, and Heats of CO_2 Adsorption of the Presented COFs

COF system	amount of D*t*ATH (%)	BET SA[a] [$m^2\ g^{-1}$]	CO_2 uptake at 273 K [mmol g^{-1}]	relative CO_2 adsorption [μmol m^{-2}]	Q_{st}[b] [kJ mol^{-1}]
amine−coCOF−H	0	2336	2.66	1.14	24.0
	25	1705	2.12	1.24	37.0
	50	811	1.60	1.97	40.4
	75	573	1.11	1.93	54.0
	100	514	1.14	2.22	72.4
amine−coCOF−OH	0	998	1.74	1.75	36.7
	25	822	1.60	1.95	47.9
	50	675	1.42	2.10	49.6
	75	581	1.27	2.19	66.0
	100	412	1.04	2.52	48.5

[a]From Ar sorption measurements. [b]At zero coverage.

but cannot be distinguished from the AA eclipsed stacking structure because of broadening of the reflections.[47,48] Further investigations were carried out with the AA eclipsed model. Pawley refinement on the simulated structure suggests a *P6/m* space group with $a = b = 29.6$ Å and $\alpha = \beta = 90°$, $\gamma = 120°$.

In general, coCOF−H appears more crystalline than coCOF−OH. Introducing the modified linker leads to a further loss in crystallinity, whereas the architecture and dimensions of the unit cell are maintained. The 100, 110, 200, and 001 reflections of 100%-amine−coCOF−OH are found at 3.4, 5.7, 6.9, and 26.3°, respectively, which suggests retention of the stacking structure discussed above. The crystallinity decreases with higher amine content (see Figure S2). The loss of crystallinity is more distinct in amine−coCOF−OH which we attribute to a loss of reversibility in the bond formation and the coexistence of different tautomeric forms which is known for COFs based on the TFG linker.[49]

Adsorption Performance. According to argon sorption measurements at 87 K, both systems show characteristic type IV isotherms that are typical for mesoporous materials (see Figure 4). Brunauer−Emmett−Teller (BET) surface areas were calculated to be 998 $m^2\ g^{-1}$ for coCOF−OH and 2336 $m^2\ g^{-1}$ for coCOF−H, which surpasses the published values for both COFs (757 and 710 $m^2\ g^{-1}$ for coCOF−OH and coCOF−H, respectively[46]). Pore size distributions (PSD) were derived from experimental data using nonlocal density functional theory and quenched solid-state functional theory calculations.[50] In coCOF−H, the experimental pore size of 2.4 nm is in agreement with the theoretical value based on the structural model. Additionally, micropores of 0.92 and 0.61 nm are observed which points to structural effects such as mismatch stacking, leading to reduced pore sizes or pore blocking. The mesopores with 2.4 nm diameter account for 65% of the pore volume, whereas the smaller micropores represent 7.4% (for 0.92 nm) and 8.3% (for 0.61 nm) of the

DOI: 10.1021/acs.chemmater.8b04643
Chem. Mater. 2019, 31, 1946−1955

total pore volume. A similar trend is observed in coCOF−OH with a broader distribution of mesopores at 2.3 nm (55% pore volume) caused by the loss of long-range order because of tautomerism (see Figure S5). The smaller pores are found at 0.91 nm (26% pore volume) and 0.61 nm (16% pore volume).

For amine-containing samples, BET surface areas decrease linearly with an increasing amount of tertiary amine. Respective values for all samples are listed in Table 1. We derived PSDs from Ar isotherms for the samples containing 50 and 100% modified linker for both systems (see Figures S4 and S5). Although the mean pore size of the pristine COFs is around 2.4 nm, additional smaller pores in the range of 1.4−1.8 nm are found for the amine-containing samples. This is in agreement with theoretical values for amine-modified pores, which vary between 1.6 and 2.2 nm depending on the amine conformation. A stochastic distribution of the different linkers in the systems along with stacking faults will lead to pores with different amounts of amine and therefore to different pore sizes, especially in the mixed systems. A broader distribution of pore sizes with more regular distribution of pore volumes is found in the 50% amine samples (see Table S2). In the 100% amine samples, two distinct pore sizes of 2.2 and 1.6 nm are found which are attributed to different pore surface architectures with amines either at the pore wall or protruding into the pore (see Figure S6).

With respect to the CO_2 sorption isotherms of both systems, a linear decrease was observed for the uptake capacity ranging from 2.66 to 1.14 mmol g^{-1} for coCOF−H (0−100% modification) and from 1.74 to 1.04 mmol g^{-1} for coCOF−OH (0−100% modification; see Table 1). Interestingly, the loss in uptake capacity with increasing amine functionalization is significantly less than the decrease of surface area. Normalizing the CO_2 uptake to the BET surface area of the samples (see Table 1) to obtain relative rather than absolute CO_2 capacities, the uptake increases from 1.14 to 2.22 μmol m^{-2} (0−100% modification) for the amine−coCOF−H. For amine−coCOF−OH, the relative CO_2 adsorption increases from 1.75 to 2.52 μmol m^{-2} (see Figure 4b). Whereas at 50% amine loading, the uptake is fairly similar for both systems (2.10 μmol m^{-2} for amine−coCOF−OH and 1.93 μmol m^{-2} for amine−coCOF−H), in the other amine loading regimes, the relative CO_2 capacity of the more polar amine−coCOF−OH distinctly surpasses amine−coCOF−H.

Even though water is present in most applications, the behavior of COFs in water sorption experiments has rarely been studied systematically. Most studies have been performed on MOFs or porous carbons that show very different behaviors. Hydrophilicity is more pronounced in the case of MOFs because of their metal sites than on the nonpolar hydrophobic surface of carbon materials. However, MOFs are often not stable in water which leads to their degradation under humid conditions.[51] COFs are expected to exhibit hydration properties that are intermediate between MOFs and carbons, where a more polar surface due to heteroatoms in the framework gives rise to a type IV sorption isotherm and a fully reversible hysteresis at lower relative pressures compared to nonpolar surfaces.

The two pristine COF systems in this study show similar behavior in water sorption measurements. The water uptake capacity is higher for amine−coCOF−H, ranging from 598 to 768 $cm^3\ g^{-1}$ (47−61 wt %) and 416−481 $cm^3\ g^{-1}$ (33 to 38 wt %). In both systems, the highest capacity is found for the 100%-amine samples and the lowest for the 50%-amine samples. This is likely due to a higher degree of disorder because of the distribution of modified and unmodified linkers in the 50%-amine samples. The adsorption isotherms of both systems show a step in the range of 0.30−0.45 p/p_0 with a strong hysteresis; the same step is found in the desorption isotherm at 0.20−0.30 p/p_0. This behavior is indicative of capillary condensation of water in the COF pores. By increasing the amine content in the samples, in both systems, the adsorption step flattens out up to an almost linear sorption isotherm in 100%-amine−coCOF−OH. This continuous pore filling might be due to a slightly higher polarity in the system. Interestingly, water sorption is not fully reversible. Fractions ranging from 6.8% (for pristine coCOF−OH) up to 11.4% (in the case of 100%-amine−coCOF−OH) of the maximum water uptake remain in the pores after desorption. The addition of amines in close proximity to the pore walls leads to higher hydrophilicity and thus increased water sorption capacities.

Isosteric heats of adsorption (Q_{st}) at zero coverage were calculated for all samples from the CO_2 sorption isotherms at 273, 288, and 298 K (see Table 1). Typical values for classical physisorption range between 8 and 25 kJ mol^{-1} for van der Waals forces and up to 50 kJ mol^{-1} for dipole−dipole interactions, whereas chemisorption is associated with heats of adsorption between 80 and 500 kJ mol^{-1}. The values obtained in our unmodified coCOFs are 24.0 kJ mol^{-1} for coCOF−H and 36.7 kJ mol^{-1} for coCOF−OH. Upon modification, the Q_{st} values increase drastically with maximum values of 72.4 kJ mol^{-1} in 100%-amine−coCOF−H and 66.0 kJ mol^{-1} in 75%-amine−coCOF−OH. Those values approach the chemisorption regime and are much higher than that for comparable COFs, such as COF-JLU2 (31 kJ mol^{-1}),[52] TRIPTA (56.77 kJ mol^{-1}),[53] [HO2C]100%-H2P−COF (43.5 kJ mol^{-1}),[27] ACOF-1 (27.6 kJ mol^{-1}),[54] TpPA−COF (34.1 kJ mol^{-1}),[55] or other porous materials such as FCTF-1 (35.0 kJ mol^{-1}),[56] MgMOF-74 (42 kJ mol^{-1}),[57] and imine-linked porous organic cages (20.4 kJ mol^{-1}).[58]

Amine-Modification of the coCOF−H Framework. To understand the improved CO_2 sorption properties of 100%-amine−coCOF−H, advanced 1D and 2D ^1H, ^{13}C, and ^{15}N solid-state NMR techniques were used to elucidate atomic-level structures and interactions in the modified COF framework and compared with findings from quantum chemical calculations. The ^{15}N chemical shift interaction is highly sensitive to local bonding environments;[59,60] however, ^{15}N NMR experiments are severely limited for low-density and low-nitrogen content materials by the low natural isotopic abundance (0.4%) and low gyromagnetic ratio of the ^{15}N nuclei. These limitations are partially overcome by dynamic nuclear polarization (DNP)-enhanced NMR spectroscopy, which uses microwave excitation of nitroxide biradical polarizing agents to achieve a potential ^{15}N sensitivity gain of $\gamma_e/\gamma_{15N} \approx 6500$.[61] Here, DNP−NMR enables the acquisition of natural-abundance ^{15}N spectra as demonstrated in Figure 5.

Although amine-functionalized nanoporous or mesoporous solids typically exhibit broad ^{15}N signals due to structural disorder,[62−64] the ^{15}N signals from the D*t*ATH linker exhibit narrow ^{15}N line shapes, which indicates relatively uniform local environments in the COF framework. The ^{15}N signals at 315 and 181 ppm are assigned to framework hydrazone (−N═) and (−NH−) moieties, respectively, as supported by quantum chemical calculations (see Figures S11, S12 and Table S4) for a coCOF−H sub-structure and literature.[59] A hydrogen bond to water causes displacement of the imine signal to lower

DOI: 10.1021/acs.chemmater.8b04643
Chem. Mater. 2019, 31, 1946−1955

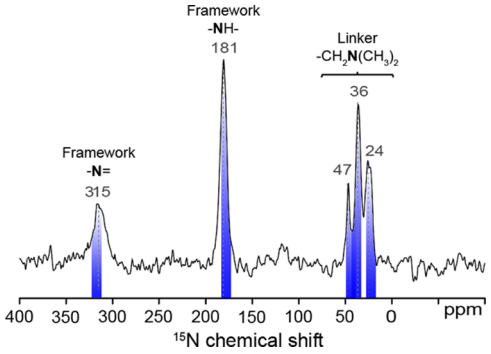

Figure 5. Solid-state 1D $^{15}N\{^{1}H\}$ DNP−CP−MAS spectra of 100%-amine−coCOF−H without CO_2 exposure. The spectrum was acquired at 9.4 T, 8 kHz MAS, 95 K, in the presence of 16 mM AMUPol biradical in 60:30:10 d_8-glycerol/D_2O/H_2O, under microwave irradiation at 263 GHz, and using cross-polarization contact times of 5 ms. Blue markings correspond to values obtained by quantum-chemical calculations (See Tables S4, S5, and S7).

frequency by approximately 12 ppm compared to the bare imine bond (see Figure S13 and Table S4). The presence of these signals, in addition to quantum chemical data, strongly suggest that after incorporation of D*t*ATH into the COF framework the hydrazone (−N═) and (−NHCO−) linkages are intact and retain an atomic structure similar to unmodified coCOF−H.

In 100%-amine−coCOF−H, there are three additional ^{15}N signals at 24, 36, and 47 ppm, which arise from the D*t*ATH linker. For tertiary amines, the ^{15}N chemical shift may be influenced by local bonding environments, which can be influenced by temperature, solvent effects, or hydrogen-bonding interactions to varying extents and which can displace ^{15}N signals by as much as 40 ppm.[60] In polar or acidic solvents, tertiary amines often exhibit partial deshielding of ^{15}N nuclei, as manifested by displacement of their isotropic chemical shifts to higher values.[60] Consequently, the ^{15}N signal at 47 ppm is assigned to protonated tertiary amine linker groups, consistent with quantum chemical calculations (see Figure S14 and Table S7). The ^{15}N signals at 24 and 36 ppm are attributed to unprotonated D*t*ATH tertiary amine moieties also on the basis of quantum-chemical calculations (Figure S13), with the former assigned to unhydrated linkers. The ^{15}N signal at 36 ppm is attributed to D*t*ATH tertiary amine moieties that interact strongly with water.

CO_2 Interactions with Amine-coCOF-H Moieties. Molecular-level insights on specific interactions between CO_2 and 100%-amine−coCOF−H are obtained from 2D $^{13}C\{^{1}H\}$-heteronuclear correlation (HETCOR) analyses that establish spatial proximities of adsorbed CO_2 and the COF sorbent. Previously, site-specific CO_2 adsorption in tertiary amide (−NHCOR)-containing mesoporous materials has been investigated by inelastic neutron spectroscopy for which subtle differences in local chemical environments are difficult to resolve.[65] By comparison, the 2D $^{13}C\{^{1}H\}$ low-temperature magic-angle-spinning (LTMAS)−HETCOR spectra (Figure 6) of 100%-amine−coCOF−H can detect and resolve atomic-level interactions of specific COF framework moieties with adsorbed water and with adsorbed CO_2.

Specifically, 2D $^{13}C\{^{1}H\}$-HETCOR methods rely on through-space dipole-dipole interactions to selectively detect ^{13}C nuclei which are in molecular-level proximity (<1 nm) to ^{1}H nuclei of both directly bound and neighboring moieties. The resulting 2D $^{13}C\{^{1}H\}$ spectrum represents a correlated intensity map that resolves spatially from molecularly near moieties on the basis of their isotropic ^{1}H and ^{13}C chemical shifts, which are sensitive to local bonding environments. For example, the 2D $^{13}C\{^{1}H\}$ HETCOR spectra in Figure 6a,b acquired for 100%-amine−coCOF−H, after exposure to ^{13}C-enriched CO_2 and then after subsequent degassing, respectively, both show intensity correlations arising from intramolecular correlations within the coCOF−H framework. These include the strong ^{13}C signals at 46, 55, and 62 ppm from alkyl carbon atoms in the D*t*ATH linker which are correlated with ^{1}H signals from alkyl protons at 2.0−3.5 ppm; and ^{13}C signals ranging from 112 to 147 ppm from aromatic

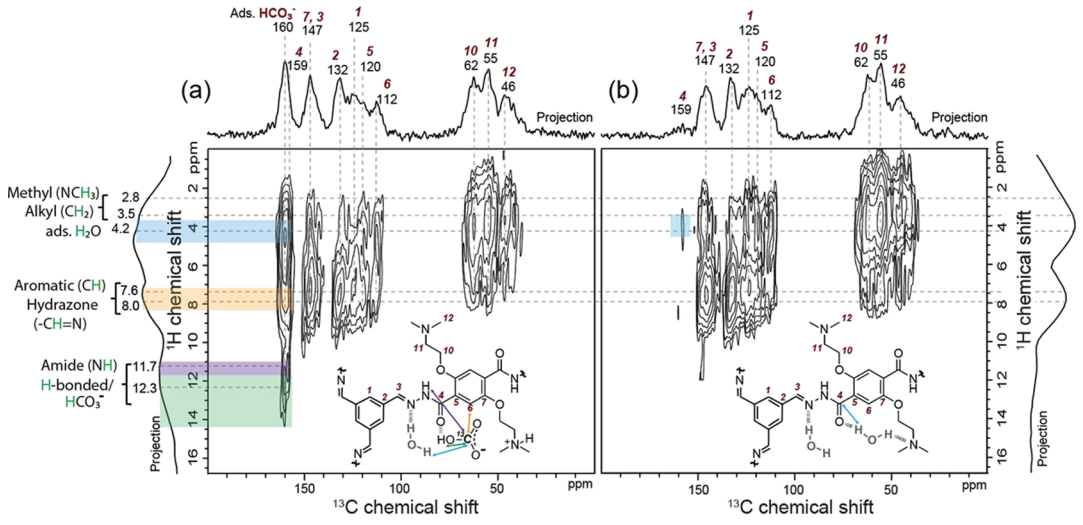

Figure 6. Solid-state 2D $^{13}C\{^{1}H\}$ LTMAS−HETCOR spectra of vacuum-dried 100%-amine−coCOF−H (a) after exposure to 100% ^{13}C-enriched CO_2 for 12 h at 1 bar pressure and 298 K and (b) after desorption of CO_2 for 48 h by vacuum heating at 0.1 bar and 363 K. The spectra were acquired at 9.4 T, 8 kHz MAS, 95 K using short cross-polarization contact times of 500 μs. 1D ^{13}C projections are shown along the horizontal axes for comparison with the 2D spectra, and 1D ^{1}H projections are shown along the vertical axes. Strong correlated ^{13}C signal intensity (ca. 160 ppm) with ^{1}H signal at 12−14 ppm establishes that CO_2 chemisorbs to form a bicarbonate (HCO_3^-) species.

DOI: 10.1021/acs.chemmater.8b04643
Chem. Mater. 2019, 31, 1946−1955

carbon atoms in the 100%-amine−coCOF−H backbone that are strongly correlated with ^{1}H signals at 7.0−8.0 ppm from aromatic protons. The framework amide moieties exhibit a ^{1}H chemical shift at 11.7 ppm, which is consistent with a 2D $^{15}N\{^{1}H\}$ DNP−HETCOR spectrum of 100%-amine−coCOF−H (Supporting Information, Figure S10b) and a 1D solution-state ^{1}H NMR spectrum of a small-molecular analogue (see the Supporting Information, compound 6). A correlated 2D intensity is also observed between the ^{13}C signal at ca. 160 ppm and a new ^{1}H signal in the range 12−14 ppm, which is assigned to intramolecular HCO_3^- interactions (green band).[66] Nearly all of the ^{13}C signals are correlated with ^{1}H intensity centered at 4.2 ppm from adsorbed H_2O. More interestingly, for 100%-amine−coCOF−H exposed to ^{13}C-enriched CO_2 (Figure 6a), the ^{13}C intensity in the range 160−164 ppm is also strongly correlated with ^{1}H signals at 4.2 and 7.0−8.0 and 11.7 ppm, which are assigned to adsorbed H_2O (blue band) and hydrazone and/or aromatic ^{1}H moieties (beige band), and amide groups (purple band), respectively. Such 2D intensity correlations unambiguously establish that chemisorption of CO_2 occurs in close molecular proximities to these moieties, which are consistent with the isotropic ^{13}C chemical shifts that have been reported for the formation of bicarbonate species in tertiary amine solutions.[67] The breadth of the ^{13}C intensity reflects a distribution of solvated neutral (160 ppm)[68] and ionic bicarbonate species (171 ppm from quantum chemical calculations, see Table S6). The 2D NMR results thus establish that HCO_3^- strongly interacts with adsorbed H_2O and amide and/or aromatic ^{1}H moieties in the 100%-amine−coCOF−H framework.

As shown by the 1D $^{13}C\{^{1}H\}$ DNP-CP MAS spectra in Figure S9a,b, the ^{13}C amide signal (orange overbar) has stronger intensity for the longest CP contact time of 5 ms. Although ^{13}C-depleted glycerol was used in the DNP solvent formulation, there is a small intensity shoulder ranging from 65 to 80 ppm from glycerol. By comparison, the 1D $^{13}C\{^{1}H\}$ LTMAS−CP MAS spectra in Figure S9c,d were acquired on vacuum-dried 100%-amine−coCOF−H upon exposure to dry 100% ^{13}C-enriched CO_2 and after subsequent degassing step. As discussed in the experimental section, these materials were characterized without DNP to minimally influence adsorbed CO_2. Under otherwise identical conditions, there is significantly more ^{13}C signal at 160 ppm for the material exposed to ^{13}C-enriched CO_2. In the 1D spectra, the adsorbed bicarbonate (red overbar) and amide have overlapping signal intensity at 160 ppm. By comparison, for the short contact time (500 μs) used in Figure 6, only the strongest $^{13}C\{^{1}H\}$ dipole-dipole-coupled moieties are expected to yield correlated intensity, which is consistent with the reduced signals from the amide moieties, the carbon atoms of which lack a directly bonded ^{1}H atom.

Despite degassing and drying the sorbent prior to CO_2 adsorption, 100%-amine−coCOF−H strongly retains adsorbed H_2O, which favors the formation of bicarbonates. Evidence for hydrogen-bonding interactions between H_2O and the framework amide (−NH−) moieties was also observed in a 2D $^{15}N\{^{1}H\}$ DNP−HETCOR spectrum (see the Supporting Information, Figure S8). After desorption of the CO_2 100% ^{13}C-enriched CO_2, the ^{13}C signal (ca. 160 ppm) from bicarbonate completely disappears. However, there are still strong intensity correlations associated with ^{13}C moieties in 100%-amine−coCOF−H and ^{1}H moieties from adsorbed H_2O at ca. 4.2 ppm (blue band) and only very weak correlated intensity associated with the amide ^{13}C signal remains at ca. 159 ppm, which is consistent with the observed water desorption behavior of the samples. The retention of H_2O in 100%-amine−coCOF−H likely contributes to the reduction in the apparent BET surface area. Stronger interactions with CO_2 are usually attributed to a higher amount of heteroatoms, mostly nitrogen and oxygen, on the pore walls of porous framework materials, because of the higher interaction affinity of the heteroatoms to CO_2.[3,69,70] In the context of the aminated COF materials, the interaction with water cannot be neglected. In addition to CO_2 adsorption functionality, the amine groups impart hydrophilicity that leads to increased water uptake by the framework. The increased network hydrophilicity promotes H_2O adsorption and deprotonation near the basic amine side chains, which promotes CO_2 coadsorption as bicarbonate species in the 100%-amine−coCOF−H pores. Note that increasing amounts of adsorbed water in the pores with increasing degree of amine functionalization is consistent with the water isotherms discussed above.

CONCLUSIONS

In this study, a mixed linker strategy was used to modify coCOF−H and coCOF−OH with a tertiary amine functionality by copolymerization of isostructural linkers. Addition of the functionalized linker species yields a higher affinity to CO_2 as shown by an increased relative CO_2 adsorption capacity, along with an increase of the heat of adsorption at zero coverage up to a value of 72.4 kJ mol^{-1}. We demonstrate by solid-state 2D $^{13}C\{^{1}H\}$ NMR analyses, supplemented by quantum chemical NMR calculations, that CO_2 sorption in the 100%-amine−coCOF−H pores proceeds via formation of a bicarbonate species adsorbed within the COF−CO_2 pores, along with water which is strongly retained. Thus, the hydrophilicity of the COF framework appears to promote increased CO_2 sorption capacity, with different hydrophilicities leading to distinctly different adsorption behaviors of water in the pores. This is likely the reason that increased extents of framework functionalization with amine species lead to increased CO_2 affinity because of the formation of bicarbonate species. Such effects are partially offset by decreased surface area because of steric effects associated with the linkers, as well as strongly retained water in the pores. Tuning the COF's inherent water sorption properties by introducing functional groups such as tertiary amines or amides that promote CO_2 solvation[71] is expected to further enhance CO_2 adsorption in porous systems.

ASSOCIATED CONTENT

Supporting Information

The Supporting Information is available free of charge on the ACS Publications website at DOI: 10.1021/acs.chemmater.8b04643.

Synthesis and methods, additional measurements and characterization, and details of quantum-chemical calculations (PDF)

AUTHOR INFORMATION

Corresponding Author

*E-mail: b.lotsch@fkf.mpg.de.

DOI: 10.1021/acs.chemmater.8b04643
Chem. Mater. 2019, 31, 1946−1955

ORCID

Gökcen Savasci: 0000-0002-6183-7715
Christian Ochsenfeld: 0000-0002-4189-6558
Bettina V. Lotsch: 0000-0002-3094-303X

Notes

The authors declare no competing financial interest.

■ ACKNOWLEDGMENTS

Financial support is gratefully acknowledged from the Max Planck Society, the ERC Starting Grant (project COF Leaf, grant number 639233), the cluster of excellence "Nanosystems Initiative München" (NIM), the Center for NanoScience (CeNS), and for the UCSB group, the U.S. National Science Foundation (award no. CBET-1335694). We thank Prof. T. Bein and Prof. W. Schnick (University of Munich, LMU) for granting access to the XRD facility and V. Duppel for the assistance with material analysis. The solid-state NMR measurements were conducted using the MRL Shared Experimental Facilities supported by the MRSEC Program of the U.S. NSF under award no. DMR 1720256, a member of the NSF-funded Materials Research Facilities Network (www.mrfn.org). Z.J.B. acknowledges funding from the BASF corporation. C.O. acknowledges also support as Max-Planck-Fellow at MPI-FKF Stuttgart.

■ REFERENCES

(1) Hug, S.; Mesch, M. B.; Oh, H.; Popp, N.; Hirscher, M.; Senker, J.; Lotsch, B. V. A fluorene based covalent triazine framework with high CO2 and H2 capture and storage capacities. *J. Mater. Chem. A* **2014**, *2*, 5928−5936.

(2) Doonan, C. J.; Tranchemontagne, D. J.; Glover, T. G.; Hunt, J. R.; Yaghi, O. M. Exceptional ammonia uptake by a covalent organic framework. *Nat. Chem.* **2010**, *2*, 235−238.

(3) Li, Z.; Feng, X.; Zou, Y.; Zhang, Y.; Xia, H.; Liu, X.; Mu, Y. A 2D azine-linked covalent organic framework for gas storage applications. *Chem. Commun.* **2014**, *50*, 13825−13828.

(4) Wan, S.; Guo, J.; Kim, J.; Ihee, H.; Jiang, D. A Belt-Shaped, Blue Luminescent, and Semiconducting Covalent Organic Framework. *Angew. Chem., Int. Ed.* **2008**, *47*, 8826−8830.

(5) Wan, S.; Guo, J.; Kim, J.; Ihee, H.; Jiang, D. A Photoconductive Covalent Organic Framework: Self-Condensed Arene Cubes Composed of Eclipsed 2D Polypyrene Sheets for Photocurrent Generation. *Angew. Chem., Int. Ed.* **2009**, *48*, 5439−5442.

(6) Dogru, M.; Handloser, M.; Auras, F.; Kunz, T.; Medina, D.; Hartschuh, A.; Knochel, P.; Bein, T. A Photoconductive Thienothiophene-Based Covalent Organic Framework Showing Charge Transfer Towards Included Fullerene. *Angew. Chem., Int. Ed.* **2013**, *52*, 2920−2924.

(7) Stegbauer, L.; Schwinghammer, K.; Lotsch, B. V. A hydrazone-based covalent organic framework for photocatalytic hydrogen production. *Chem. Sci.* **2014**, *5*, 2789−2793.

(8) Cote, A. P.; Benin, A. I.; Ockwig, N. W.; O'Keeffe, M.; Matzger, A. J.; Yaghi, O. M. <Porous, Crystalline, Covalent Organic Frameworks Yaghi 2005.pdf>. *Science* **2005**, *310*, 1166−1170.

(9) Ding, S.-Y.; Wang, W. Covalent organic frameworks (COFs): from design to applications. *Chem. Soc. Rev.* **2013**, *42*, 548−568.

(10) Tilford, R. W.; Mugavero, S. J.; Pellechia, P. J.; Lavigne, J. J. Tailoring Microporosity in Covalent Organic Frameworks. *Adv. Mater.* **2008**, *20*, 2741−2746.

(11) Stegbauer, L.; Zech, S.; Savasci, G.; Banerjee, T.; Podjaski, F.; Schwinghammer, K.; Ochsenfeld, C.; Lotsch, B. V. Tailor-Made Photoconductive Pyrene-Based Covalent Organic Frameworks for Visible-Light Driven Hydrogen Generation. *Adv. Energy Mater.* **2018**, *8*, 1703278.

(12) Nagai, A.; Guo, Z.; Feng, X.; Jin, S.; Chen, X.; Ding, X.; Jiang, D. Pore surface engineering in covalent organic frameworks. *Nat. Commun.* **2011**, *2*, 536.

(13) Li, Z.-J.; Ding, S.-Y.; Xue, H.-D.; Cao, W.; Wang, W. Synthesis of -C═N- linked covalent organic frameworks via the direct condensation of acetals and amines. *Chem. Commun.* **2016**, *52*, 7217−7220.

(14) Chen, X.; Addicoat, M.; Jin, E.; Xu, H.; Hayashi, T.; Xu, F.; Huang, N.; Irle, S.; Jiang, D. Designed synthesis of double-stage two-dimensional covalent organic frameworks. *Sci. Rep.* **2015**, *5*, 14650.

(15) Zhang, Y.; Shen, X.; Feng, X.; Xia, H.; Mu, Y.; Liu, X. Covalent organic frameworks as pH responsive signaling scaffolds. *Chem. Commun.* **2016**, *52*, 11088−11091.

(16) Kang, Z.; Peng, Y.; Qian, Y.; Yuan, D.; Addicoat, M. A.; Heine, T.; Hu, Z.; Tee, L.; Guo, Z.; Zhao, D. Mixed Matrix Membranes (MMMs) Comprising Exfoliated 2D Covalent Organic Frameworks (COFs) for Efficient CO2 Separation. *Chem. Mater.* **2016**, *28*, 1277−1285.

(17) Olajire, A. A. Recent advances in the synthesis of covalent organic frameworks for CO2 capture. *J. CO2 Util.* **2017**, *17*, 137−161.

(18) Chowdhury, F. A.; Yamada, H.; Higashii, T.; Goto, K.; Onoda, M. CO2 Capture by Tertiary Amine Absorbents: A Performance Comparison Study. *Ind. Eng. Chem. Res.* **2013**, *52*, 8323−8331.

(19) Ko, Y. G.; Shin, S. S.; Choi, U. S. Primary, secondary, and tertiary amines for CO2 capture: Designing for mesoporous CO2 adsorbents. *J. Colloid Interface Sci.* **2011**, *361*, 594−602.

(20) Zhang, R.; Liang, Z.; Liu, H.; Rongwong, W.; Luo, X.; Idem, R.; Yang, Q. Study of Formation of Bicarbonate Ions in CO2-Loaded Aqueous Single 1DMA2P and MDEA Tertiary Amines and Blended MEA−1DMA2P and MEA−MDEA Amines for Low Heat of Regeneration. *Ind. Eng. Chem. Res.* **2016**, *55*, 3710−3717.

(21) Rochelle, G. T. Amine Scrubbing for CO2 Capture. *Science* **2009**, *325*, 1652−1654.

(22) Wang, J.; Huang, L.; Yang, R.; Zhang, Z.; Wu, J.; Gao, Y.; Wang, Q.; O'Hare, D.; Zhong, Z. Recent advances in solid sorbents for CO2 capture and new development trends. *Energy Environ. Sci.* **2014**, *7*, 3478−3518.

(23) Titirici, M.-M.; White, R. J.; Brun, N.; Budarin, V. L.; Su, D. S.; del Monte, F.; Clark, J. H.; MacLachlan, M. J. Sustainable carbon materials. *Chem. Soc. Rev.* **2015**, *44*, 250−290.

(24) Liu, J.; Thallapally, P. K.; McGrail, B. P.; Brown, D. R.; Liu, J. Progress in adsorption-based CO2 capture by metal−organic frameworks. *Chem. Soc. Rev.* **2012**, *41*, 2308−2322.

(25) Sumida, K.; Rogow, D. L.; Mason, J. A.; McDonald, T. M.; Bloch, E. D.; Herm, Z. R.; Bae, T.-H.; Long, J. R. Carbon Dioxide Capture in Metal−Organic Frameworks. *Chem. Rev.* **2012**, *112*, 724−781.

(26) Zhang, X.; Lu, J.; Zhang, J. Porosity Enhancement of Carbazolic Porous Organic Frameworks Using Dendritic Building Blocks for Gas Storage and Separation. *Chem. Mater.* **2014**, *26*, 4023−4029.

(27) Huang, N.; Chen, X.; Krishna, R.; Jiang, D. Two-Dimensional Covalent Organic Frameworks for Carbon Dioxide Capture through Channel-Wall Functionalization. *Angew. Chem.* **2015**, *127*, 3029−3033.

(28) Kizzie, A. C.; Wong-Foy, A. G.; Matzger, A. J. Effect of Humidity on the Performance of Microporous Coordination Polymers as Adsorbents for CO2 Capture. *Langmuir* **2011**, *27*, 6368−6373.

(29) Liu, J.; Wang, Y.; Benin, A. I.; Jakubczak, P.; Willis, R. R.; LeVan, M. D. CO2/H2O Adsorption Equilibrium and Rates on Metal−Organic Frameworks: HKUST-1 and Ni/DOBDC. *Langmuir* **2010**, *26*, 14301−14307.

(30) Liang, Z.; Marshall, M.; Chaffee, A. L. CO2 Adsorption-Based Separation by Metal Organic Framework (Cu-BTC) versus Zeolite (13X). *Energy Fuels* **2009**, *23*, 2785−2789.

(31) Krishnamurthy, S.; Rao, V. R.; Guntuka, S.; Sharratt, P.; Haghpanah, R.; Rajendran, A.; Amanullah, M.; Karimi, I. A.; Farooq,

DOI: 10.1021/acs.chemmater.8b04643
Chem. Mater. 2019, 31, 1946−1955

S. CO2 capture from dry flue gas by vacuum swing adsorption: A pilot plant study. *AIChE J.* **2014**, *60*, 1830−1842.
(32) Webley, P. A. Adsorption technology for CO2 separation and capture: a perspective. *Adsorption* **2014**, *20*, 225−231.
(33) Kong, X.; Scott, E.; Ding, W.; Mason, J. A.; Long, J. R.; Reimer, J. A. CO2 Dynamics in a Metal−Organic Framework with Open Metal Sites. *J. Am. Chem. Soc.* **2012**, *134*, 14341−14344.
(34) Lin, L.-C.; Kim, J.; Kong, X.; Scott, E.; McDonald, T. M.; Long, J. R.; Reimer, J. A.; Smit, B. Understanding CO2 Dynamics in Metal−Organic Frameworks with Open Metal Sites. *Angew. Chem., Int. Ed.* **2013**, *52*, 4410−4413.
(35) McDonald, T. M.; Mason, J. A.; Kong, X.; Bloch, E. D.; Gygi, D.; Dani, A.; Crocellà, V.; Giordanino, F.; Odoh, S. O.; Drisdell, W. S.; Vlaisavljevich, B.; Dzubak, A. L.; Poloni, R.; Schnell, S. K.; Planas, N.; Lee, K.; Pascal, T.; Wan, L. F.; Prendergast, D.; Neaton, J. B.; Smit, B.; Kortright, J. B.; Gagliardi, L.; Bordiga, S.; Reimer, J. A.; Long, J. R. Cooperative insertion of CO2 in diamine-appended metal-organic frameworks. *Nature* **2015**, *519*, 303.
(36) Wilson, P. J.; Bradley, T. J.; Tozer, D. J. Hybrid exchange-correlation functional determined from thermochemical data and ab initio potentials. *J. Chem. Phys.* **2001**, *115*, 9233−9242.
(37) Jensen, F. The Basis Set Convergence of Spin−Spin Coupling Constants Calculated by Density Functional Methods. *J. Chem. Theory Comput.* **2006**, *2*, 1360−1369.
(38) Perdew, J. P.; Burke, K.; Ernzerhof, M. Generalized Gradient Approximation Made Simple. *Phys. Rev. Lett.* **1996**, *77*, 3865−3868.
(39) Grimme, S.; Antony, J.; Ehrlich, S.; Krieg, H. A consistent and accurate ab initio parametrization of density functional dispersion correction (DFT-D) for the 94 elements H-Pu. *J. Chem. Phys.* **2010**, *132*, 154104.
(40) Weigend, F.; Häser, M.; Patzelt, H.; Ahlrichs, R. RI-MP2: optimized auxiliary basis sets and demonstration of efficiency. *Chem. Phys. Lett.* **1998**, *294*, 143−152.
(41) Weigend, F. Accurate Coulomb-fitting basis sets for H to Rn. *Phys. Chem. Chem. Phys.* **2006**, *8*, 1057−1065.
(42) TURBOMOLE V7.1 2017. http://www.turbomole.com (accessed Jan 30, 2019), a development of University of Karlsruhe and Forschungszentrum Karlsruhe GmbH, 1989−2007. TURBOMOLE GmbH, since 2007.
(43) Ahlrichs, R.; Bär, M.; Häser, M.; Horn, H.; Kölmel, C. Electronic structure calculations on workstation computers: The program system turbomole. *Chem. Phys. Lett.* **1989**, *162*, 165−169.
(44) Kussmann, J.; Ochsenfeld, C. Pre-selective screening for matrix elements in linear-scaling exact exchange calculations. *J. Chem. Phys.* **2013**, *138*, 134114.
(45) Kussmann, J.; Ochsenfeld, C. Preselective Screening for Linear-Scaling Exact Exchange-Gradient Calculations for Graphics Processing Units and General Strong-Scaling Massively Parallel Calculations. *J. Chem. Theory Comput.* **2015**, *11*, 918−922.
(46) Uribe-Romo, F. J.; Doonan, C. J.; Furukawa, H.; Oisaki, K.; Yaghi, O. M. Crystalline Covalent Organic Frameworks with Hydrazone Linkages. *J. Am. Chem. Soc.* **2011**, *133*, 11478−11481.
(47) Spitler, E. L.; Koo, B. T.; Novotney, J. L.; Colson, J. W.; Uribe-Romo, F. J.; Gutierrez, G. D.; Clancy, P.; Dichtel, W. R. A 2D Covalent Organic Framework with 4.7-nm Pores and Insight into Its Interlayer Stacking. *J. Am. Chem. Soc.* **2011**, *133*, 19416−19421.
(48) Haase, F.; Gottschling, K.; Stegbauer, L.; Germann, L. S.; Gutzler, R.; Duppel, V.; Vyas, V. S.; Kern, K.; Dinnebier, R. E.; Lotsch, B. V. Tuning the stacking behaviour of a 2D covalent organic framework through non-covalent interactions. *Mater. Chem. Front.* **2017**, *1*, 1354−1361.
(49) Stegbauer, L.; Hahn, M. W.; Jentys, A.; Savasci, G.; Ochsenfeld, C.; Lercher, J. A.; Lotsch, B. V. Tunable Water and CO2 Sorption Properties in Isostructural Azine-Based Covalent Organic Frameworks through Polarity Engineering. *Chem. Mater.* **2015**, *27*, 7874−7881.
(50) Lowell, S.; Shields, J. E.; Thomas, M. A.; Thommes, M. *Characterization of Porous Solids and Powders: Surface Area, Pore Size and Density*; Springer, 2012.
(51) Datta, S. J.; Khumnoon, C.; Lee, Z. H.; Moon, W. K.; Docao, S.; Nguyen, T. H.; Hwang, I. C.; Moon, D.; Oleynikov, P.; Terasaki, O.; Yoon, K. B. CO_2 capture from humid flue gases and humid atmosphere using a microporous coppersilicate. *Science* **2015**, *350*, 302−306.
(52) Zhongping, L.; Yongfeng, Z.; Xiao, F.; Xuesong, D.; Yongcun, Z.; Xiaoming, L.; Ying, M. An Azine-Linked Covalent Organic Framework: Synthesis, Characterization and Efficient Gas Storage. *Chem.—Eur. J.* **2015**, *21*, 12079−12084.
(53) Gomes, R.; Bhaumik, A. A new triazine functionalized luminescent covalent organic framework for nitroaromatic sensing and CO2 storage. *RSC Adv.* **2016**, *6*, 28047−28054.
(54) Shan, M.; Seoane, B.; Rozhko, E.; Dikhtiarenko, A.; Clet, G.; Kapteijn, F.; Gascon, J. Azine-Linked Covalent Organic Framework (COF)-Based Mixed-Matrix Membranes for CO2/CH4 Separation. *Chem.—Eur. J.* **2016**, *22*, 14467−14470.
(55) Kandambeth, S.; Mallick, A.; Lukose, B.; Mane, M. V.; Heine, T.; Banerjee, R. Construction of crystalline 2D covalent organic frameworks with remarkable chemical (acid/base) stability via a combined reversible and irreversible route. *J. Am. Chem. Soc.* **2012**, *134*, 19524−19527.
(56) Zhao, Y.; Yao, K. X.; Teng, B.; Zhang, T.; Han, Y. A perfluorinated covalent triazine-based framework for highly selective and water−tolerant CO2 capture. *Energy Environ. Sci.* **2013**, *6*, 3684−3692.
(57) Mason, J. A.; Sumida, K.; Herm, Z. R.; Krishna, R.; Long, J. R. Evaluating metal−organic frameworks for post-combustion carbon dioxide capture via temperature swing adsorption. *Energy Environ. Sci.* **2011**, *4*, 3030−3040.
(58) Lei, Z.; Long, X.; Cheng, H.; Wenlong, L.; Wei, H.; Yichang, P. From Discrete Molecular Cages to a Network of Cages Exhibiting Enhanced CO2 Adsorption Capacity. *Angew. Chem., Int. Ed.* **2017**, *56*, 7787−7791.
(59) Radek, M.; Antonin, L.; Erkki, K.; Elina, S.; Jaromir, T. 15N NMR Spectroscopy in Structural Analysis: An Update (2001−2005). *Curr. Org. Chem.* **2007**, *11*, 1154−1205.
(60) Martin, G. J.; Martin, M. L.; Gouesnard, J.-P. *^{15}N-NMR Spectroscopy*; Springer-Verlag, 1981.
(61) Kobayashi, T.; Gupta, S.; Caporini, M. A.; Pecharsky, V. K.; Pruski, M. Mechanism of Solid-State Thermolysis of Ammonia Borane: A 15N NMR Study Using Fast Magic-Angle Spinning and Dynamic Nuclear Polarization. *J. Phys. Chem. C* **2014**, *118*, 19548−19555.
(62) Pinto, M. L.; Mafra, L.; Guil, J. M.; Pires, J.; Rocha, J. Adsorption and Activation of CO2 by Amine-Modified Nanoporous Materials Studied by Solid-State NMR and 13CO2 Adsorption. *Chem. Mater.* **2011**, *23*, 1387−1395.
(63) Chen, C.-H.; Shimon, D.; Lee, J. J.; Didas, S. A.; Mehta, A. K.; Sievers, C.; Jones, C. W.; Hayes, S. E. Spectroscopic Characterization of Adsorbed 13CO2 on 3-Aminopropylsilyl-Modified SBA15 Mesoporous Silica. *Environ. Sci. Technol.* **2017**, *51*, 6553−6559.
(64) Moschetta, E. G.; Sakwa-Novak, M. A.; Greenfield, J. L.; Jones, C. W. Post-Grafting Amination of Alkyl Halide-Functionalized Silica for Applications in Catalysis, Adsorption, and 15N NMR Spectroscopy. *Langmuir* **2015**, *31*, 2218−2227.
(65) Benson, O.; da Silva, I.; Argent, S. P.; Cabot, R.; Savage, M.; Godfrey, H. G. W.; Yan, Y.; Parker, S. F.; Manuel, P.; Lennox, M. J.; Mitra, T.; Easun, T. L.; Lewis, W.; Blake, A. J.; Besley, E.; Yang, S.; Schröder, M. Amides Do Not Always Work: Observation of Guest Binding in an Amide-Functionalized Porous Metal−Organic Framework. *J. Am. Chem. Soc.* **2016**, *138*, 14828−14831.
(66) Nebel, H.; Neumann, M.; Mayer, C.; Epple, M. On the Structure of Amorphous Calcium Carbonate—A Detailed Study by Solid-State NMR Spectroscopy. *Inorg. Chem.* **2008**, *47*, 7874−7879.
(67) Kortunov, P. V.; Siskin, M.; Baugh, L. S.; Calabro, D. C. In Situ Nuclear Magnetic Resonance Mechanistic Studies of Carbon Dioxide Reactions with Liquid Amines in Non-aqueous Systems: Evidence for the Formation of Carbamic Acids and Zwitterionic Species. *Energy Fuels* **2015**, *29*, 5940−5966.

DOI: 10.1021/acs.chemmater.8b04643
Chem. Mater. 2019, 31, 1946−1955

(68) Seravalli, J.; Ragsdale, S. W. 13C NMR Characterization of an Exchange Reaction between CO and CO2 Catalyzed by Carbon Monoxide Dehydrogenase. *Biochemistry* **2008**, *47*, 6770−6781.
(69) Yongfei, Z.; Ruqiang, Z.; Yanli, Z. Covalent Organic Frameworks for CO2 Capture. *Adv. Mater.* **2016**, *28*, 2855−2873.
(70) Sharma, A.; Malani, A.; Medhekar, N. V.; Babarao, R. CO2 adsorption and separation in covalent organic frameworks with interlayer slipping. *CrystEngComm* **2017**, *19*, 6950−6963.
(71) Lee, H. M.; Youn, I. S.; Saleh, M.; Lee, J. W.; Kim, K. S. Interactions of CO2 with various functional molecules. *Phys. Chem. Chem. Phys.* **2015**, *17*, 10925−10933.

DOI: 10.1021/acs.chemmater.8b04643
Chem. Mater. 2019, 31, 1946−1955